Ultrahigh coulombic efficiency electrolyte enables Li||SPAN batteries with superior cycling performance

Haodong Liu[1], John Holoubek[1], Hongyao Zhou[1], Amanda Chen[1], Naijen Chang[1], Zhaohui Wu[1], Sicen Yu[1], Qizhang Yan[1], Xing Xing[1], Yejing Li[1], Tod A. Pascal[1,2*], Ping Liu[1,2*]

[1] Department of NanoEngineering, University of California San Diego, 9500 Gilman Drive, La Jolla, CA, 92093, USA

[2] Sustainable Power and Energy Center, University of California San Diego, 9500 Gilman Drive, La Jolla, CA, 92093, USA

Corresponding authors: piliu@eng.ucsd.edu (P. Liu); tpascal@eng.ucsd.edu (T. Pascal)

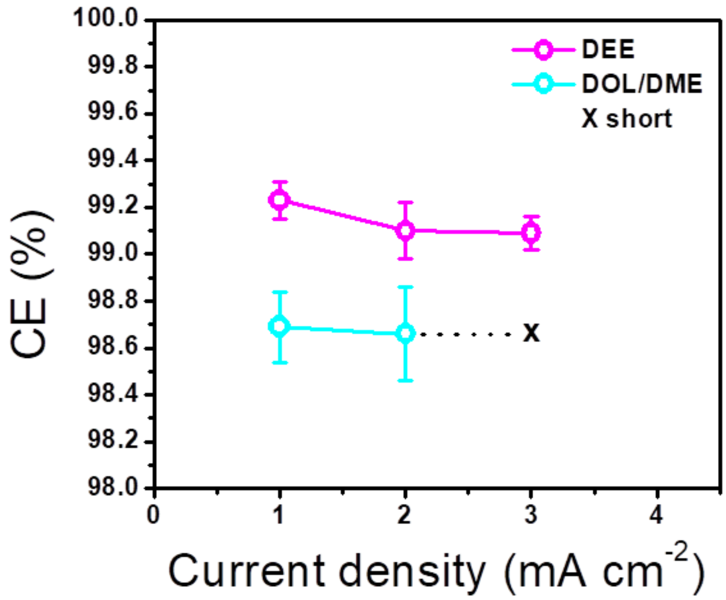

Figure S1. The comparison of Li-metal plating/stripping coulombic efficiencies in 1 M LiFSI/DOL-DME, and 1 M LiFSI/DEE electrolytes at various current densities.

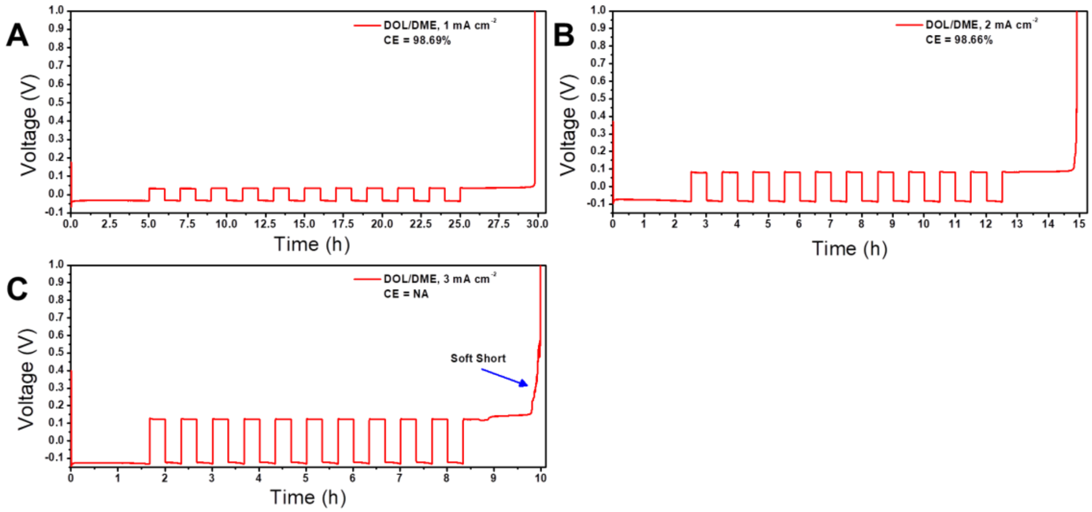

Figure S2. The plating/stripping voltage profiles of Li||Cu cell cycled in 1 M LiFSI/DOL-DME electrolyte. Prior to the test, a condition cycle was carried out on all the cells, in this step a Li film was first deposited onto the Cu foil at 0.5 mA cm^{-2} for 10 hours, and then fully stripped to 1 V. Another Li film (5 mAh cm^{-2}) was deposited again, only 1 mAh cm^{-2} capacity of Li film was stripped and plated for 10 cycles. Finally, the Li film was fully stripped to 1 V. The current density during this test was (A) 1 mA cm^{-2}; (B) 2 mA cm^{-2}; (C) 3 mA cm^{-2}.

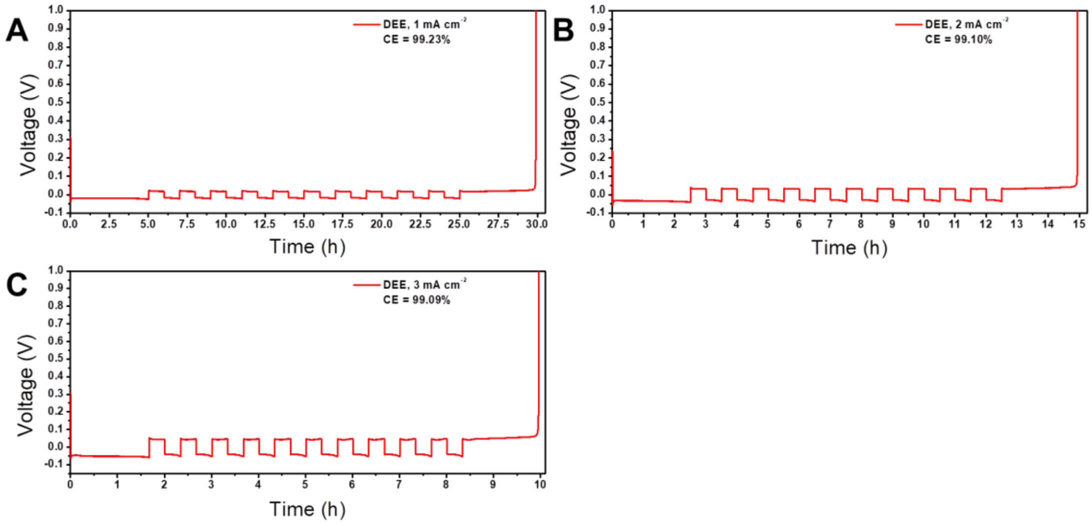

Figure S3. The plating/stripping voltage profiles of Li||Cu cell cycled in 1 M LiFSI/DEE electrolyte. Prior to the test, a condition cycle was carried out on all the cells, in this step a Li film was first deposited onto the Cu foil at 0.5 mA cm^{-2} for 10 hours, and then fully stripped to 1 V. Another Li film (5 mAh cm^{-2}) was deposited again, only 1 mAh cm^{-2} capacity of Li film was stripped and plated for 10 cycles. Finally, the Li film was fully stripped to 1 V. The current density during this test was (A) 1 mA cm^{-2}; (B) 2 mA cm^{-2}; (C) 3 mA cm^{-2}.

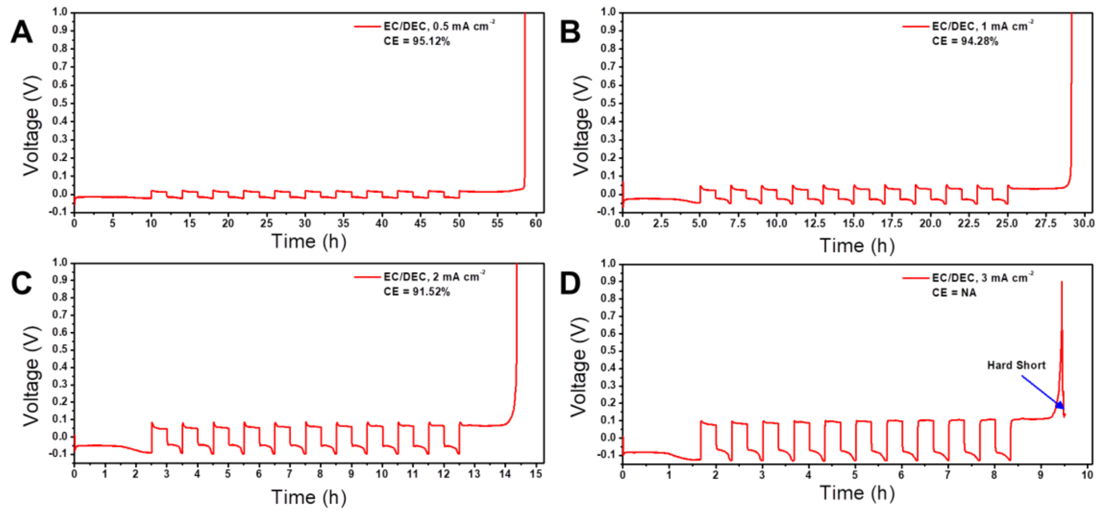

Figure S4. The plating/stripping voltage profiles of Li||Cu cell cycled in 1 M LiFSI/EC-DEC electrolyte. Prior to the test, a condition cycle was carried out on all the cells, in this step a Li film was first deposited onto the Cu foil at 0.5 mA cm^{-2} for 10 hours, and then fully stripped to 1 V. Another Li film (5 mAh cm^{-2}) was deposited again, only 1 mAh cm^{-2} capacity of Li film was stripped and plated for 10 cycles. Finally, the Li film was fully stripped to 1 V. The current density during this test was (A) 0.5 mA cm^{-2}; (B) 1 mA cm^{-2}; (C) 2 mA cm^{-2}; (D) 3 mA cm^{-2}.

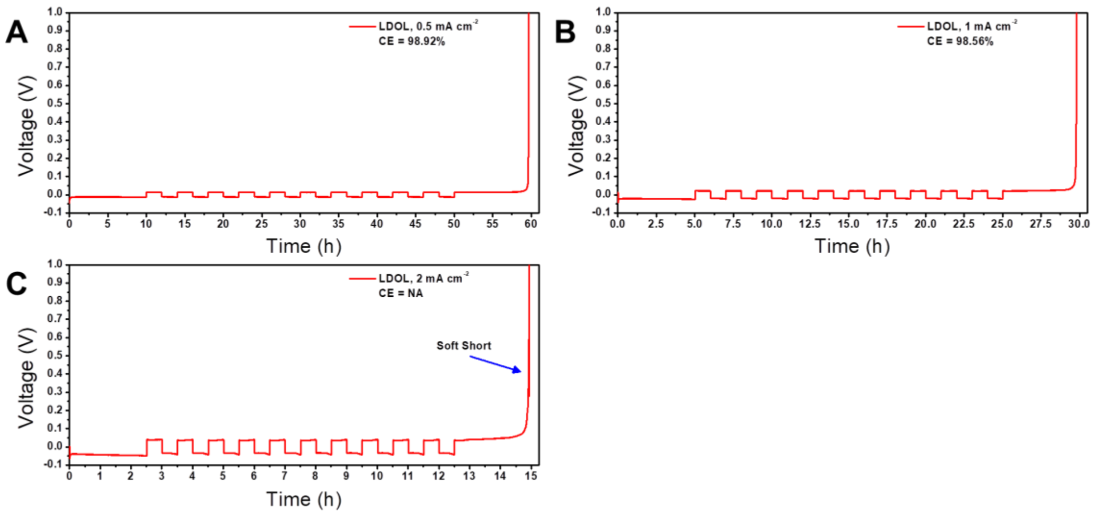

Figure S5. The plating/stripping voltage profiles of Li||Cu cell cycled in 0.47 M LiFSI/DOL-BTFE electrolyte. Prior to the test, a condition cycle was carried out on all the cells, in this step a Li film was first deposited onto the Cu foil at 0.5 mA cm^{-2} for 10 hours, and then fully stripped to 1 V. Another Li film (5 mAh cm^{-2}) was deposited again, only 1 mAh cm^{-2} capacity of Li film was stripped and plated for 10 cycles. Finally, the Li film was fully stripped to 1 V. The current density during this test was (A) 0.5 mA cm^{-2}; (B) 1 mA cm^{-2}; (C) 2 mA cm^{-2}.

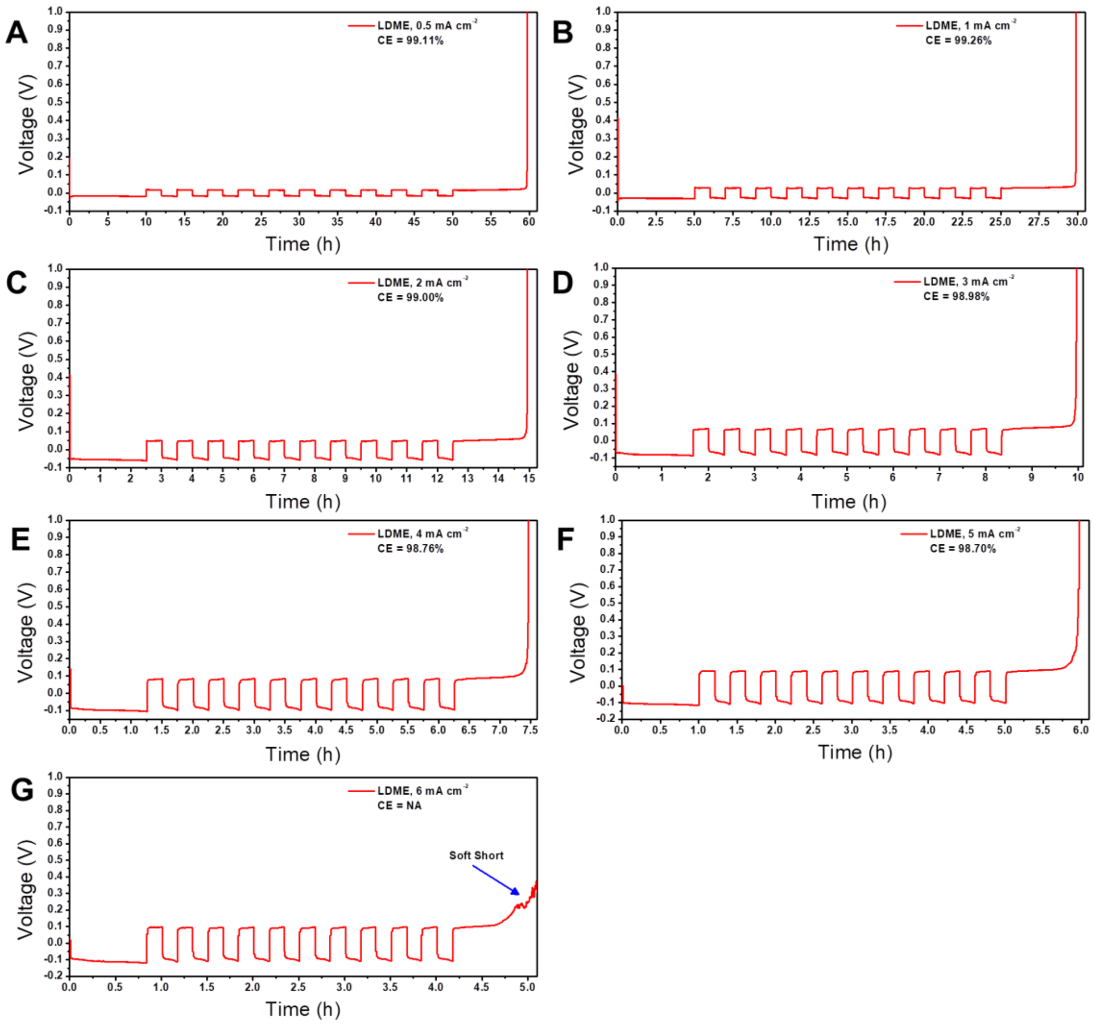

Figure S6. The plating/stripping voltage profiles of Li||Cu cell cycled in 2.54 M LiFSI/DME-BTFE electrolyte. Prior to the test, a condition cycle was carried out on all the cells, in this step a Li film was first deposited onto the Cu foil at 0.5 mA cm^{-2} for 10 hours, and then fully stripped to 1 V. Another Li film (5 mAh cm^{-2}) was deposited again, only 1 mAh cm^{-2} capacity of Li film was stripped and plated for 10 cycles. Finally, the Li film was fully stripped to 1 V. The current density during this test was (A) 0.5 mA cm^{-2}; (B) 1 mA cm^{-2}; (C) 2 mA cm^{-2}; (D) 3 mA cm^{-2}; (E) 4 mA cm^{-2}; (F) 5 mA cm^{-2}; (G) 6 mA cm^{-2}.

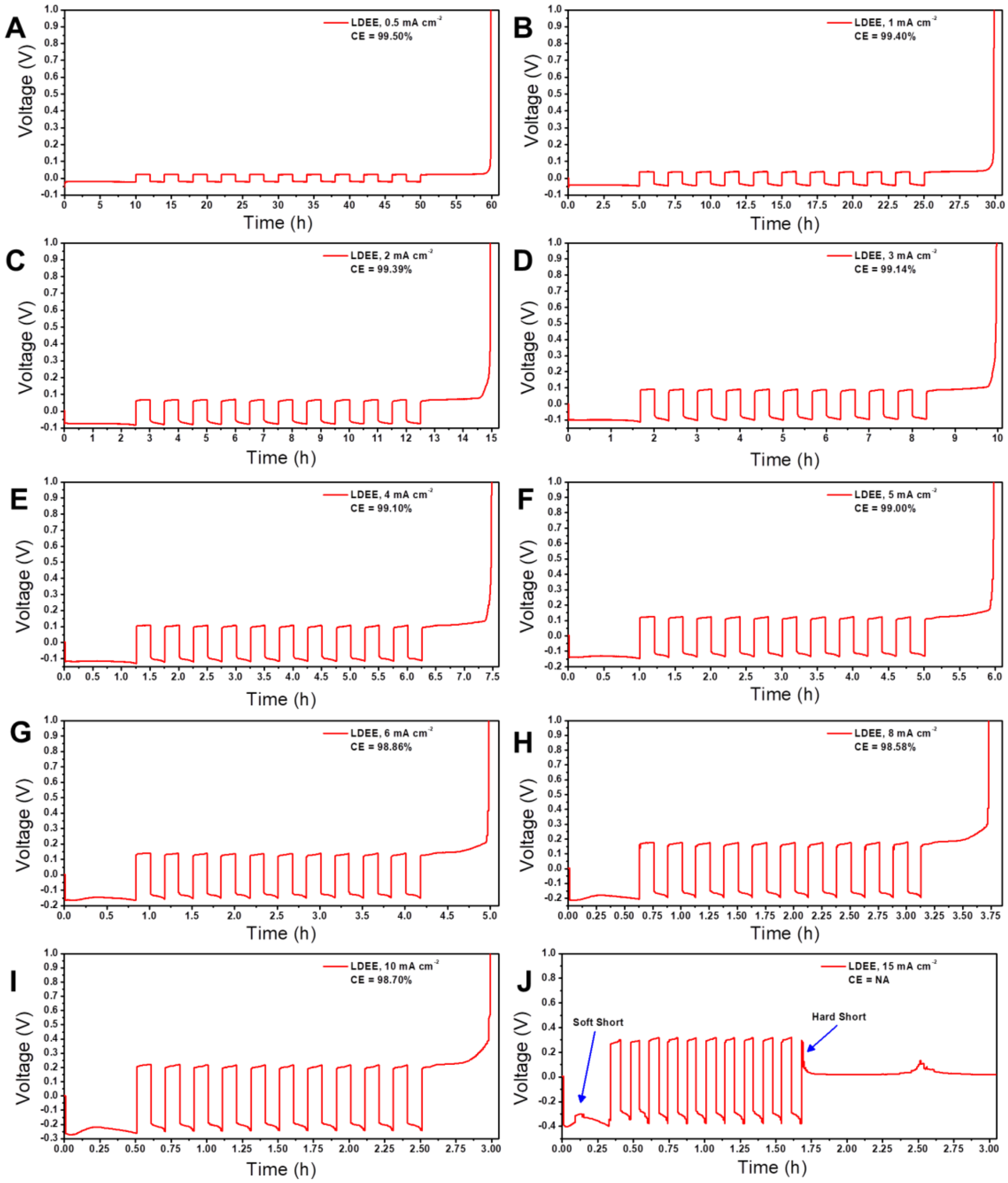

Figure S7. The plating/stripping voltage profiles of Li||Cu cell cycled in 1.8 M LiFSI/DEE-BTFE electrolyte. Prior to the test, a condition cycle was carried out on all the cells, in this step a Li film was first deposited onto the Cu foil at 0.5 mA cm^{-2} for 10 hours, and then fully stripped to 1 V. Another Li film (5 mAh cm^{-2}) was deposited again, only 1 mAh cm^{-2} capacity of Li film was stripped and plated for 10 cycles. Finally, the Li film was fully stripped to 1 V. The current density during this test was (A) 0.5 mA cm^{-2}; (B) 1 mA cm^{-2}; (C) 2 mA cm^{-2}; (D) 3 mA cm^{-2}; (E) 4 mA cm^{-2}; (F) 5 mA cm^{-2}; (G) 6 mA cm^{-2}; (H) 8 mA cm^{-2}; (I) 10 mA cm^{-2}; (J) 15 mA cm^{-2}.

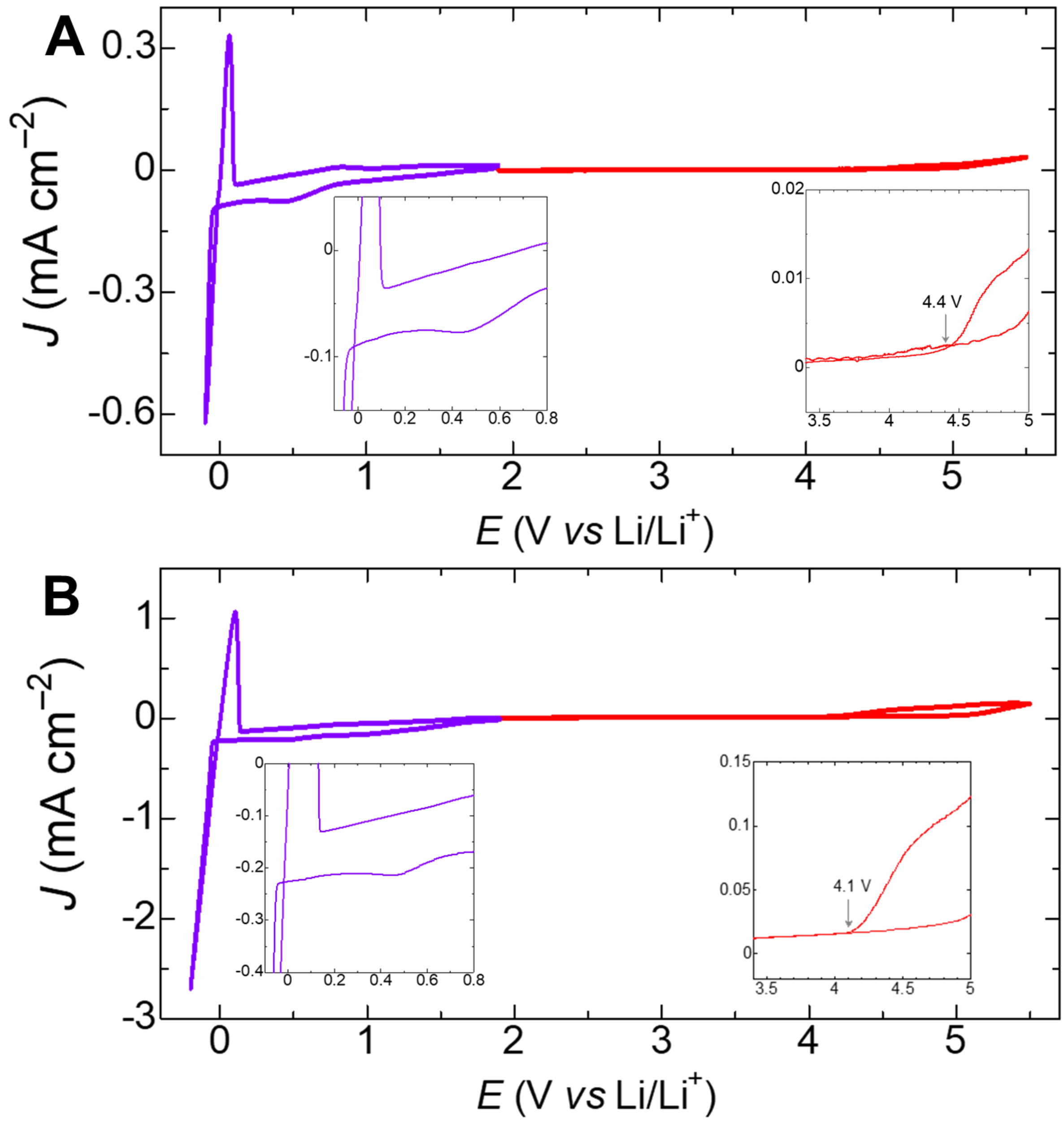

Figure S8. Reduction and oxidation stabilities for different electrolytes as evaluated on Cu and Al electrodes, respectively. At a scanning rate of 5 mV s^{-1}. (A) 9 M LiFSI/DEE electrolyte. (B) 1.8 M LiFSI/DEE electrolyte.

Electrochemical window: A three-electrodes cell was used to perform cyclic voltammetry, where the working electrode is Cu or Al foil, the reference and counter electrodes are Li metal foil. Cu working electrode was used at the reductive scan (–0.1~1.9 V vs. Li/Li^{+}). The scan rate was 5 mV s^{-1}. The scan range of –0.2~1.9 V was used for the electrolyte with BTFE, because the Li plating potential shifted to the negative side. Al working electrode was used at the oxidative scan (1.9~5.5 V vs. Li/Li^{+}). The scan rate was 5 mV s^{-1}. Before the measurement, the Al working electrode was swept between 1.9~5.5 V at a fast scan rate (100 mV s^{-1}) for 10 cycles to clean and passivate the electrode surface.

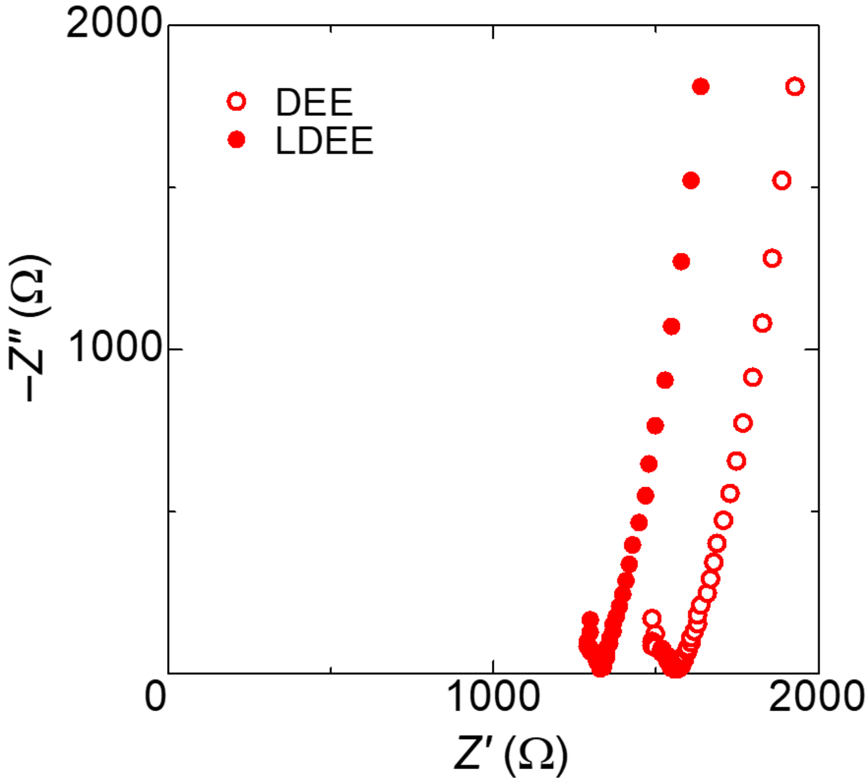

Figure S9. Electrochemical impedance spectroscopy for measuring conductivity of the electrolyte. 9 M LiFSI/DEE electrolyte (DEE), and 1.8 M LiFSI/DEE electrolyte (LDEE). Conductivity measurement: The electrolyte was placed between two mirror-finished glassy carbon electrodes with active diameter of 3.0 mm. The distance between the electrodes was 2.0 mm. An alternating voltage of 10 mV was applied between the electrodes at the frequency from 5 MHz to 100 Hz to obtain the impedance spectra. The measurement was performed at room temperature (25 °C).

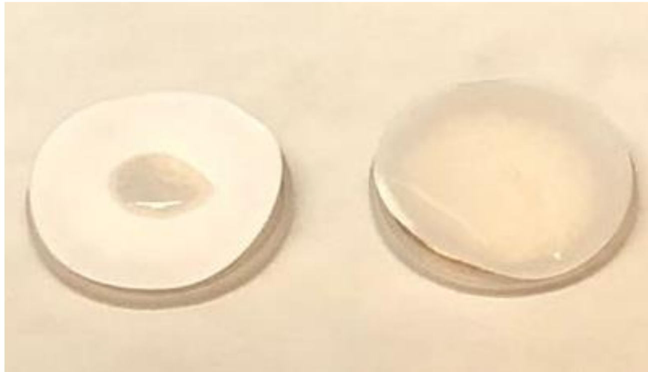

Figure S10. Wettability tests of 9 M LiFSI/DEE and 1.8 M LiFSI/DEE-BTFE electrolytes on Celgard separator.

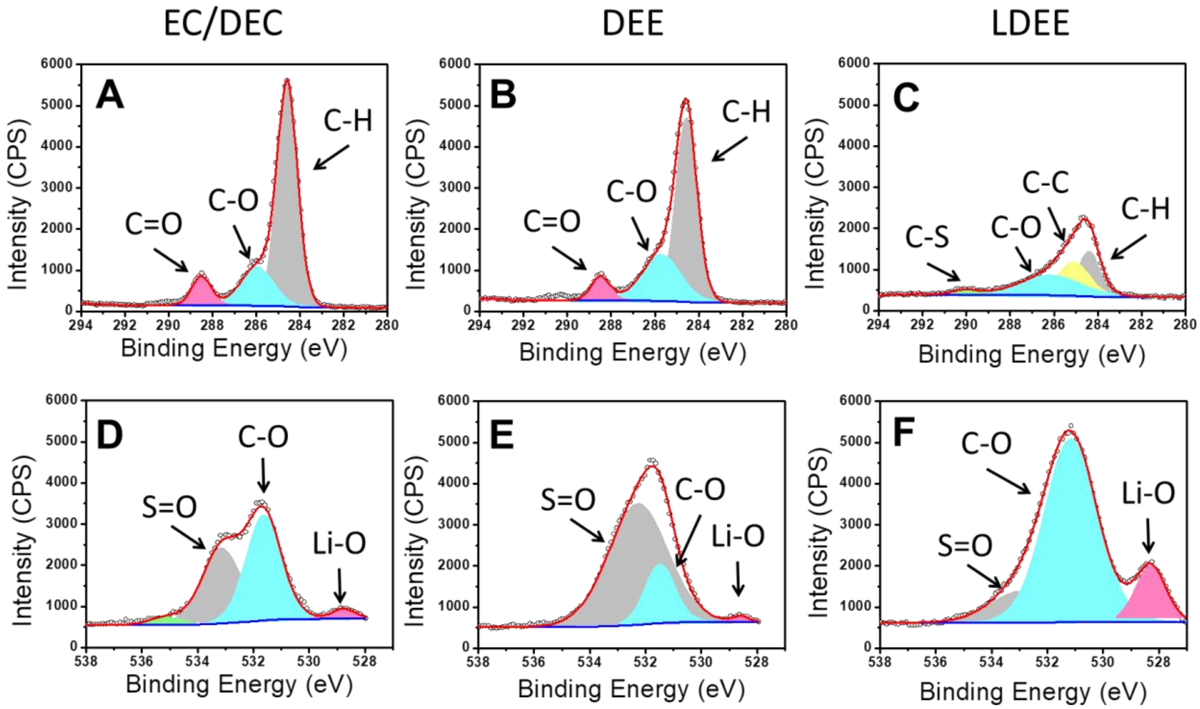

Figure S11. XPS analyses of Cu electrode on its 70th deposition. (A) C 1s region of Cu electrode from 1 M LiFSI/EC-DEC electrolyte. (B) C 1s region of Cu electrode from 1 M LiFSI/DEE electrolyte. (C) C 1s region of Cu electrode from 1.8 M LiFSI/DEE-BTFE electrolyte. (D) O 1s region of Cu electrode from 1 M LiFSI/EC-DEC electrolyte. (E) O 1s region of Cu electrode from 1 M LiFSI/DEE electrolyte. (F) O 1s region of Cu electrode from 1.8 M LiFSI/DEE-BTFE electrolyte. At 0.5 mA cm^{-2} for 1 mAh cm^{-2}.

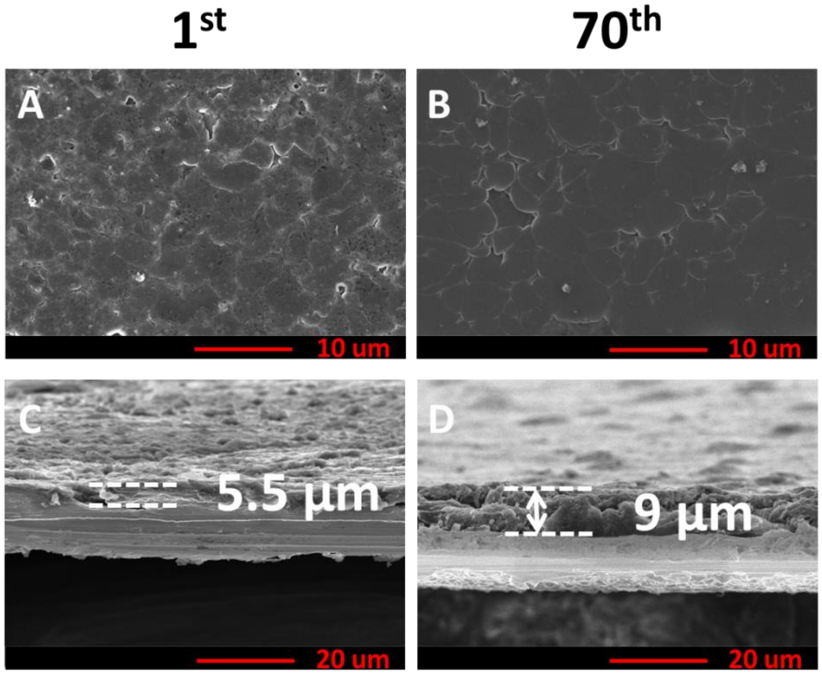

Figure S12. SEM images of Cu electrode from 1.8 M LiFSI/DEE-BTFE electrolyte. Top views: (A) 1st deposition. (B) 70th deposition. Cross sectional views: (C) 1st deposition. (D) 70th deposition. At 0.5 mA cm^{-2} for 1 mAh cm^{-2}.

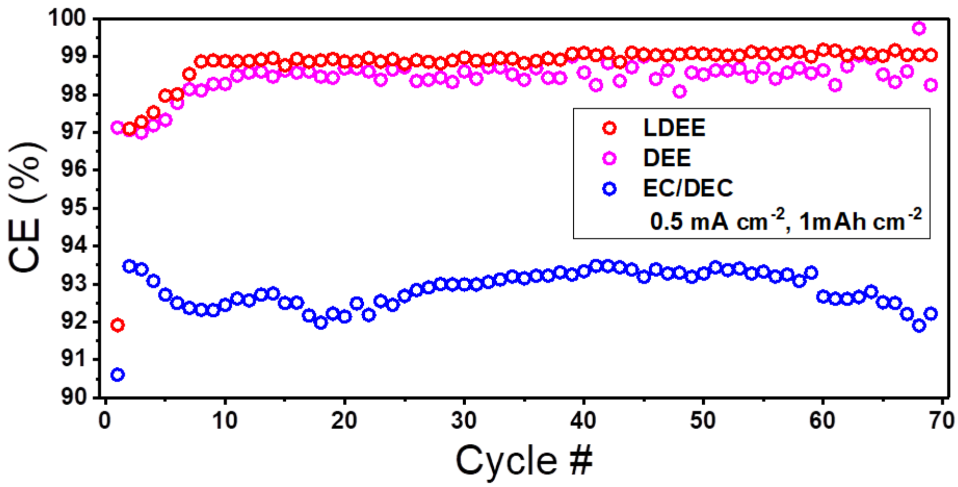

Figure S13. Coulombic efficiencies of Li||Cu cells cycled in 1.8 M LiFSI/DEE-BTFE, 1 M LiFSI/DEE, and 1 M LiFSI/EC-DEC electrolytes at 0.5 mA cm^{-2} for 1 mAh cm^{-2}.

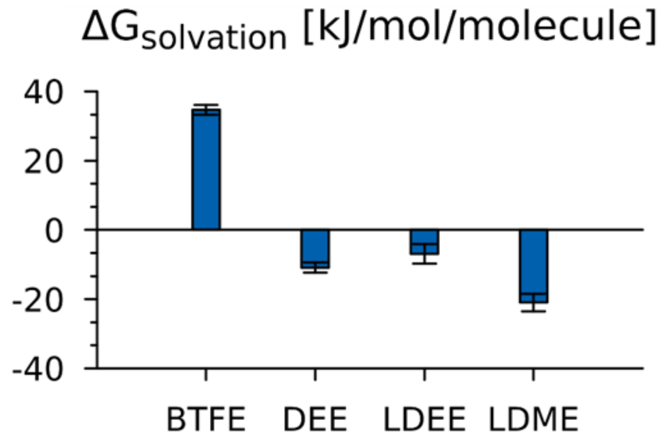

Figure S14: LiFSI Free energy of solvation for the indicated solvents/mixtures. Data for LiFSI in 1.8M DEE, 1.8M LDEE and 2.5M LDME is presented. Data for an isolated LiFSI in pure BTFE (i.e. infinite dilution limit) is also presented as a reference. The errorbars represent the uncertainty in our calculations (standard deviation).

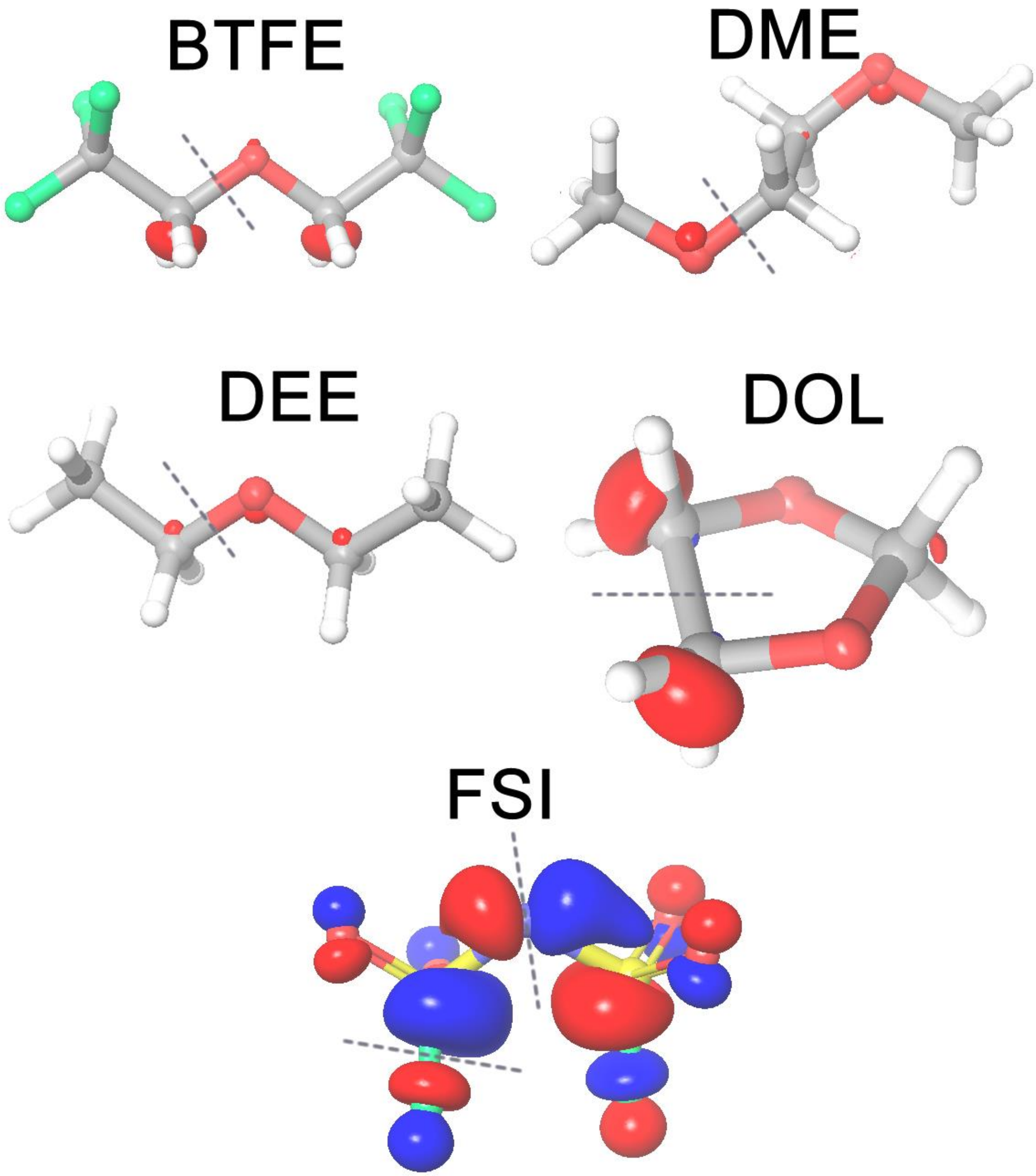

Figure S15. Electron density plot of the lowest unoccupied molecular orbitals (LUMOs) of the various molecules, evaluated at the B3LYP/aug-cc-pVTZ level of theory. In all cases, the LUMOs are anti-bonding states and the dashed lines are indicative of the chemical bonds with the most anti-bonding character. These bonds will be significantly weakened and will likely cleave when the LUMO is occupied at reductive potentials.

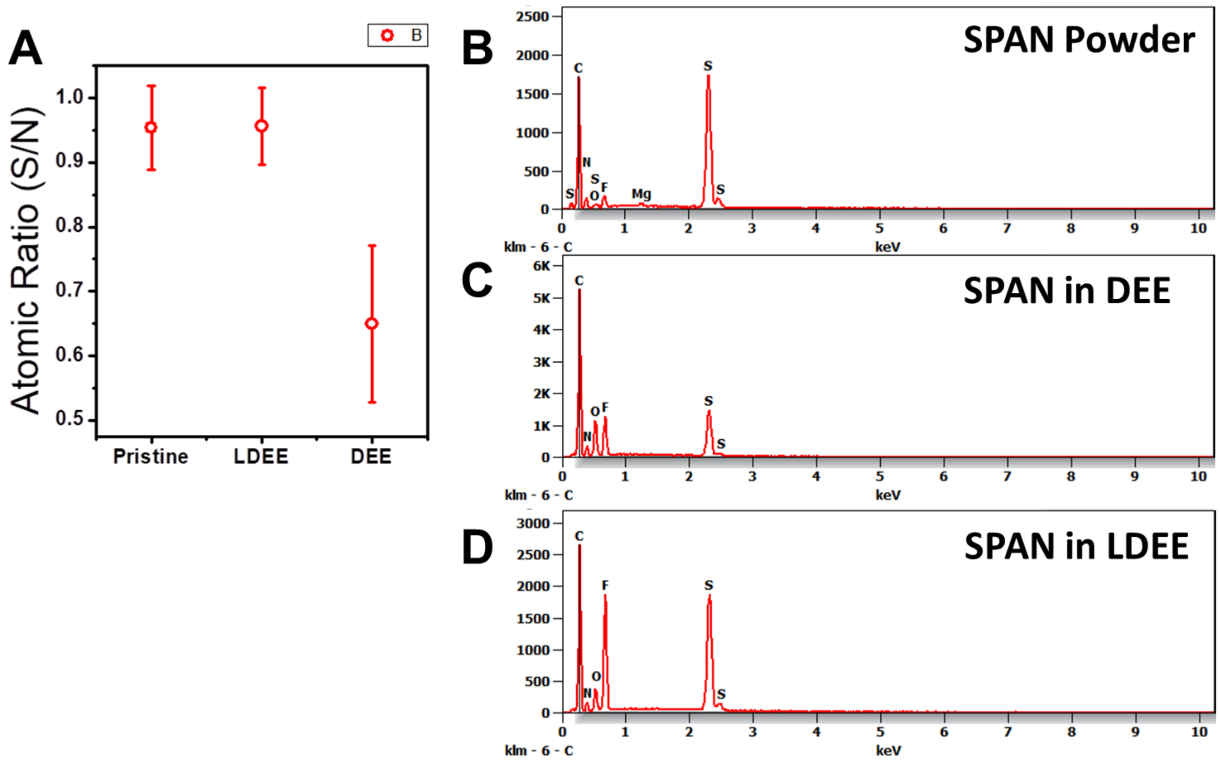

Figure S16. (A) Statistic S/N ratio results of SPAN. EDS spectra of: (B) pristine SPAN powders. (C) SPAN electrodes cycled in 1 M LiFSI/DEE. At 0.5 mA cm^{-2}, after 650 cycles. (D) SPAN electrodes cycled in 1.8 M LiFSI/DEE-BTFE. At 0.5 mA cm^{-2}, after 650 cycles.

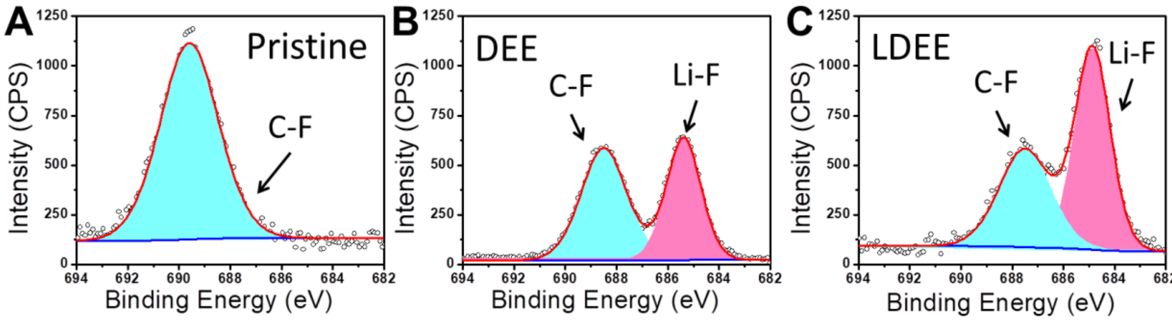

Figure S17. XPS analyses of SPAN: (A) F 1s region of pristine SPAN powders. (B) F 1s region of SPAN after cycling in 1 M LiFSI/DEE electrolyte for 650 cycles. (C) F 1s region of SPAN after cycling in 1.8 M LiFSI/DEE-BTFE electrolyte for 650 cycles. At 0.5 mA cm^{-2}.

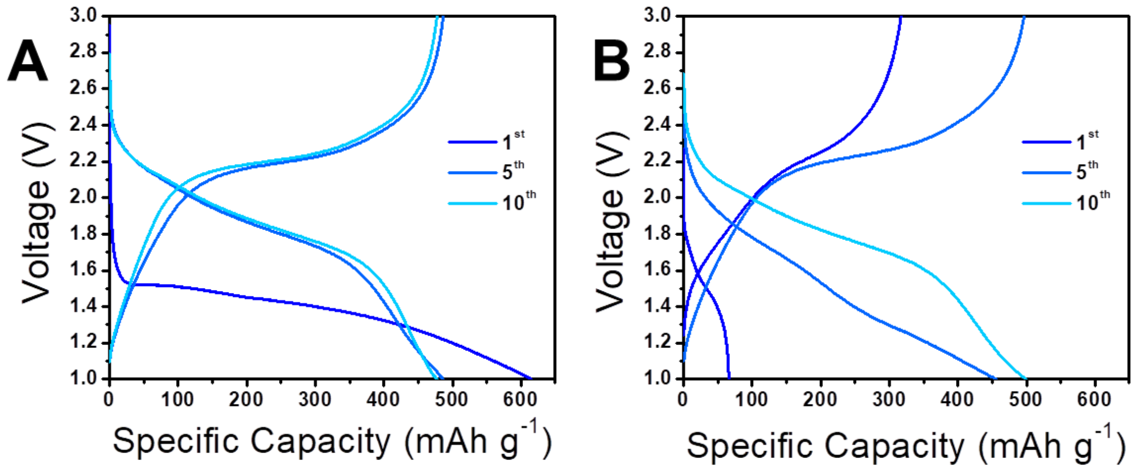

Figure S18. Charge/discharge voltage profiles of SPAN: (A) In 1 M LiFSI/EC-DEC electrolyte. (B) In 1.8 M LiFSI/DEE-BTFE electrolyte. At 0.875 mA cm^{-2}, between 1 V and 3 V. The lithium chips are 40 μm.

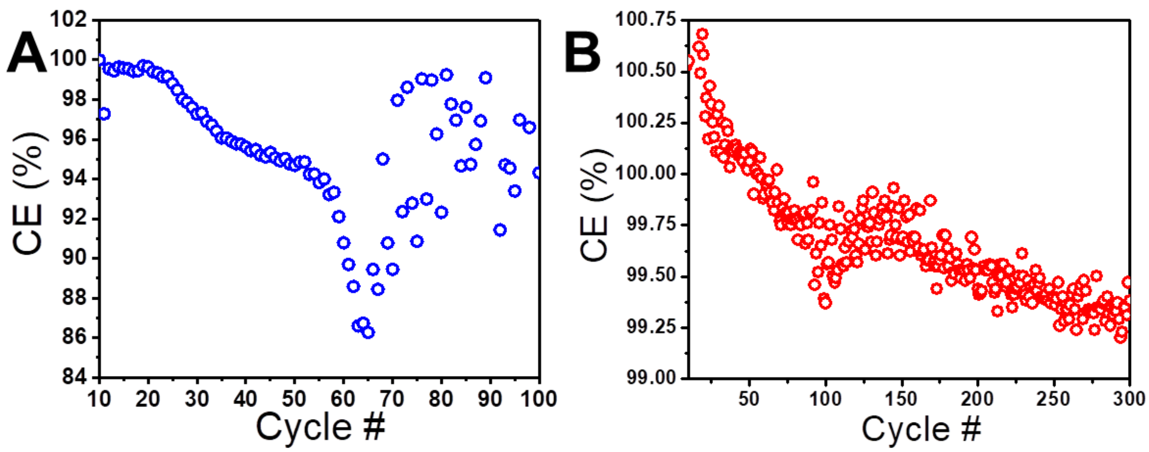

Figure S19. CEs of Li||SPAN full cells. (A) In 1 M LiFSI/EC-DEC electrolyte. (B) In 1.8 M LiFSI/DEE-BTFE electrolyte. At 1.75 mA cm^{-2}, between 1 V and 3 V. The lithium chips are 40 µm.

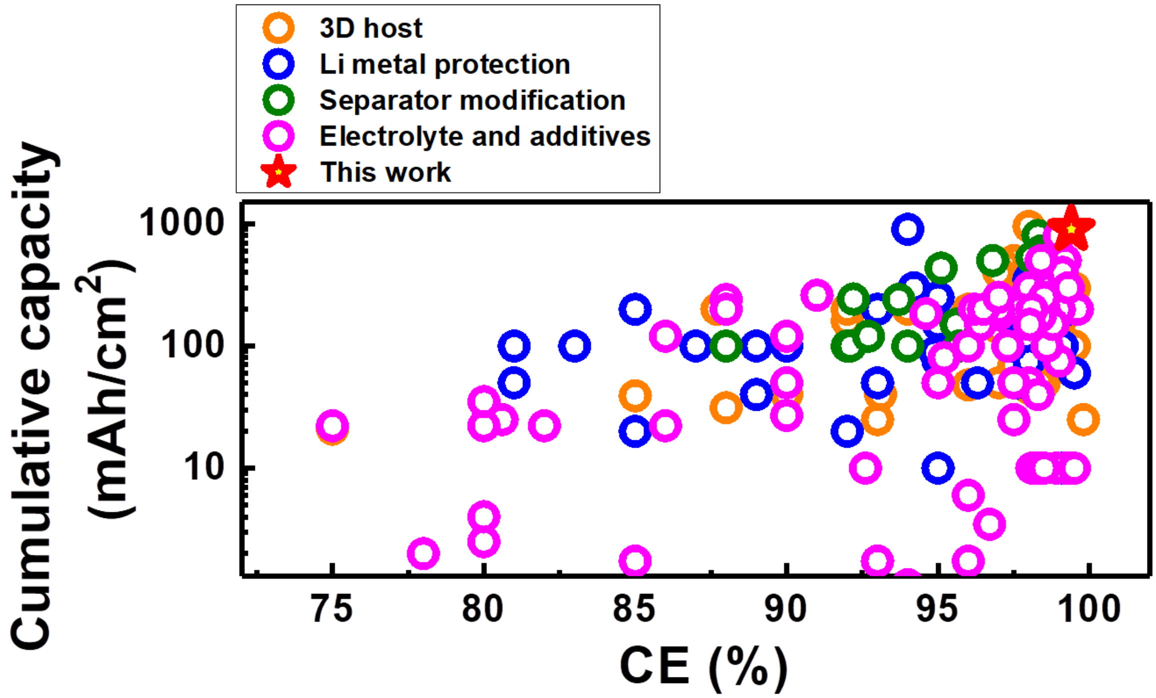

Figure S20. Summary of lithium metal anode coulombic efficiencies and lifespan from literatures.

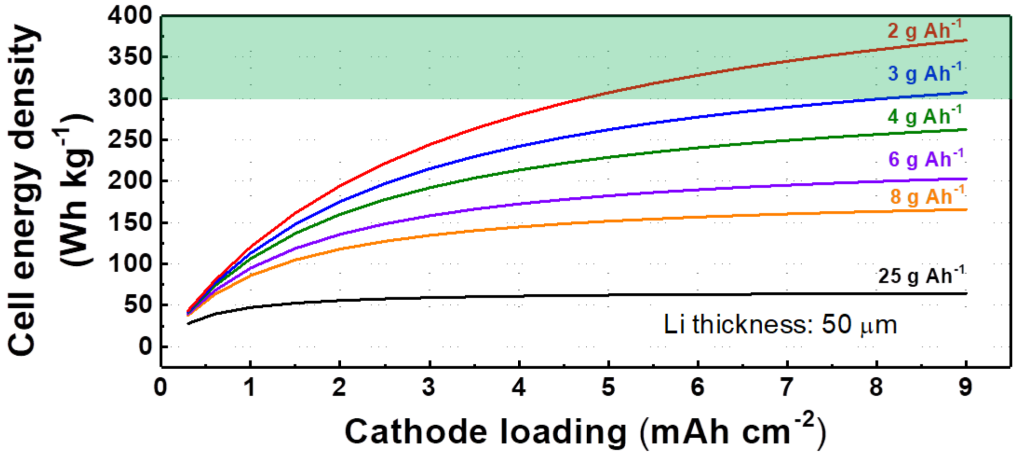

Figure S21. Calculated cell energy density of a 70 × 41.5 mm Li||SPAN pouch cell with a 50-μm Li-metal anode and 32 layers of cathodes at various cathode loadings and various electrolyte contents. The region of the graph above the 300 Wh kg^{-1} goal is shaded.

Table S1. Detail composition of electrolytes.

Electrolyte	Molar ratio	Mass ratio	Molality (mol kg^{-1})
LiFSI/EC/DEC	0.2:1.14:0.85	0.374:1:1	1
LiFSI/DOL/DME	0.2:1.35:1.11	0.374:1:1	1
LiFSI/DEE	0.1:1.35	0.187:1	1
LiFSI/DEE/BTFE	0.9:1.35:2.20	1.684:1:4	1.8
LiFSI/DME/BTFE	1.32:1.35:2.20	2.476:1.216:4	2.54
LiFSI/DOL/BTFE	0.24:1.35:2.20	0.441:1:4	0.47

Table S2. Summary of lithium metal anode coulombic efficiencies with different strategies.

3D host							
Tile of literature	Strategy	Electrolyte	Current (mA cm^{-2})	Capacity (mAh cm^{-2})	Cycle #	Cumulative Capacity (mAh)	CE
Li_2O-Reinforced Cu Nanoclusters as Porous Structure for Dendrite-Free and Long-Lifespan Lithium Metal Anode	Li_2O–Cu porous anode	1 M $LiPF_6$-EC/DMC + 2 vol% FEC	0.5	1	150	150	97%
A Scalable 3D Li metal Anode	Multifunctional 3D Li host	1 M $LiPF_6$-EC/DMC + 2 wt% VC + 0.02 M $LiNO_3$	0.25	0.5	300	150	98.37%
			0.5	1	210	210	98.11%
			1	1	200	200	97.90%
			2	2	100	200	97.05%
Vacuum distillation derived 3D porous current collector for stable lithium–metal batteries	3D porous Cu current collector	1 M $LiPF_6$-EC/DEC (1:1 vol.)	1.04	0.26	80	20.8	75%
			0.52	0.26	120	31.2	88%
Selective Deposition and Stable Encapsulation of Lithium through Heterogeneous Seeded Growth	Hollow carbon spheres with gold nanoparticle seed inside	1 M $LiPF_6$-EC/DEC (1:1 vol.) + 10% FEC + 1 % VC	0.5	1	300	300	98%
Lithiophilic Cu–Ni Core–shell Nanowire Network as a Stable Host for Improving Lithium Anode Performance	3D Cu-Ni core-shell nanowire network	1 M $LiPF_6$-EC/DEC (1:1 vol.)	2	2	100	200	92%
Interconnected hollow carbon nanospheres for stable lithium metal anodes	Interconnected hollow carbon nanospheres	1 m LiTFSI in DOL/DME with 1% $LiNO_3$ and 100×10^{-3} m Li_2S_8	0.25	1	150	150	99.0%
			0.5	1	150	150	98.5%
Prestoring Lithium into Stable 3D Nickel Foam Host as Dendrite-Free Lithium Metal Anode	Ni foam as a stable host	1 M $LiPF_6$-EC/DMC/EMC (1:1:1 vol.)	1	1	100	100	89%
Free-Standing Copper Nanowire Network Current Collector for Improving Lithium Anode Performance	Cu nanowire network	1 M $LiPF_6$-EC/EMC (2:5 wt.) with VC additives	1	1	50	50	93%
3D lithium metal embedded within lithiophilic porous matrix for stable lithium metal batteries	Porous carbon with ZnO quantum dots	1 M $LiPF_6$-EC/DMC + 1wt% FEC	0.5	1	80	40	90%
A carbon-based 3D current collector with surface protection for Li metal anode	Carbon nanotube 3D host	1 M $LiPF_6$-EC/DEC (1:1 vol.)	1	2	80	160	92%
Lithiophilic Sites in Doped Graphene Guide Uniform Lithium Nucleation for Dendrite‐Free Lithium Metal Anodes	N‐doped graphene	1.0 m LiTFSI in DOL/DME with 5% $LiNO_3$	0.5	1	150	150	98.50%
Enhanced Stability of Lithium Metal Anode by using a 3D Porous Nickel Substrate	3D Porous Nickel Substrate	LiFSI in DMC (mol ratio 0.51:1.1)	2	1	70	70	97.5%
Dendrite‐Free Lithium Deposition Induced by Uniformly Distributed Lithium Ions for Efficient Lithium Metal Batteries	3D glass fiber cloth	1 m LiTFSI in DOL/DME with 2% $LiNO_3$	0.5	0.5	90	45	98%
Dual-Phase Lithium Metal Anode Containing a Polysulfide-Induced Solid Electrolyte Interphase and Nanostructured Graphene Framework for Lithium–Sulfur Batteries	Nanostructured graphene framework	1 m LiTFSI in DOL/DME with 1% $LiNO_3$ and 0.1 M Li_2S_8	0.5	0.5	100	50	97%
Direct growth of 3D host on Cu foil for stable lithium metal anode	3D host	1 M LiTFSI in DOL/DME with 1 wt% $LiNO_3$	1	1	250	250	99%
Stable Li Plating/Stripping Electrochemistry Realized by a Hybrid Li Reservoir in Spherical Carbon Granules with 3D Conducting Skeletons	three-dimensional conducting skeleton	LiTFSI in DOL/DME with 1wt% $LiNO_3$	0.5	2	475	950	98%
Conductive Nanostructured Scaffolds Render Low Local Current Density to Inhibit Lithium Dendrite Growth	unstacked graphene " drum " and dual‐salt electrolyte	0.75 m LiTFSI in DOL and 1.5 m LiFSI in DME 2:1 (volume ratio)	0.5	0.5	50	25	93%
Chemical Dealloying Derived 3D Porous Current Collector for Li Metal Anodes	A 3D porous Cu current collector	1 m LiTFSI in DOL/DME with 1% $LiNO_3$	0.5	1	250	250	97%
			1	1	140	140	97%
A facile annealing strategy achieving in-situ controllable Cu_2O nanoparticles decorated copper foil as current	Cu_2O nanoparticles on Cu foil	1 m LiTFSI in DOL/DME with 1% $LiNO_3$	1	1	200	200	99.1%

collector for stable lithium metal anode							
Lithiophilic-lithiophobic gradient interfacial layer for a highly stable lithium metal anode	CNT with various ZnO loadings layer	0.6 M LiTFSI dissolved in 1:1 w/w DOL/DME + 0.4 M $LiNO_3$	2	3	100	300	99.50%
Unique 3D nanoporous/macroporous structure Cu current collector for dendrite-free lithium deposition	3D conductive current collectors	1 M LiTFSI in DOL/DME (1:1 by volume) with 2 wt% $LiNO_3$	1	1	200	200	98%
A Versatile Strategy to Fabricate 3D Conductive Frameworks for Lithium Metal Anodes	3D conductive current collectors	1M $LiPF_6$ in EC/DEC	0.5	1	200	200	94%
Accommodating lithium into 3D current collectors with a submicron skeleton towards long-life lithium metal anodes	3D Cu foil	1 m LiTFSI in DOL/DME with 1% $LiNO_3$ and 0.005 M Li_2S_8	0.5	1	50	50	98.5%
Vertically Grown Edge‐Rich Graphene Nanosheets for Spatial Control of Li Nucleation	Edge‐Rich Graphene Nanosheets	1 m LiTFSI in DOL/DME with 2% $LiNO_3$	1	1	200	200	97.6%
Oxygen-rich carbon nanotube networks for enhanced lithium metal anode	Oxygen-rich carbon nanotube networks	1 M LiTFSI in DOL/DME (1:1 by volume) with 1 wt% $LiNO_3$	1	2	200	400	99%
Regulating Li deposition by constructing LiF-rich host for dendrite-free lithium metal anode	An artificial LiF host	1 m LiTFSI in DOL/DME	1	1	10	10	98.5%
A synergistic strategy for stable lithium metal anodes using 3D fluorine-doped graphene shuttle-implanted porous carbon networks	3D porous carbon networks	1 m LiTFSI in DOL/DME with 2% $LiNO_3$	0.5	1	300	300	99%
			2	1	150	150	98%
Three-dimensional ordered macroporous Cu current collector for lithium metal anode: Uniform nucleation by seed crystal	three-dimensionally ordered macroporous	1 M LiTFSI in DOL/DME	0.5	0.5	80	40	93.1%
Interlayer Lithium Plating in Au Nanoparticles Pillared Reduced Graphene Oxide for Lithium Metal Anodes	Au Nanoparticles Pillared Reduced Graphene Oxide	1 m LiTFSI in DOL/DME with 1% $LiNO_3$	0.5	2	200	400	98.70%
Efficient and stable cycling of lithium metal enabled by a conductive carbon primer layer	conductive carbon primer layer	1 M $LiPF_6$ in EC/EMC 3:7	0.5	0.39	100	39	85%
Highly stable lithium metal battery with an applied three-dimensional mesh structure interlayer	three-dimensional mesh	1 M $LiPF_6$-EC/DEC (1:1 vol.)	1	1	50	50	98.35%
Robust Expandable Carbon Nanotube Scaffold for Ultrahigh‐Capacity Lithium‐Metal Anodes	carbon nanotube paper with deposited Li metal	1 m LiTFSI in DOL/DME	1	5	100	500	97.5%
AlF_3-Modified carbon nanofibers as a multifunctional 3D interlayer for stable lithium metal anodes	AlF_3-Modified carbon nanofibers	1 M $LiPF_6$ in EC/DMC with 10% FEC	1	1	450	450	97.2%
A substrate-influenced three-dimensional unoriented dispersion pathway for dendrite-free lithium metal anodes	3D Cu + MnO_2	1 m LiTFSI in DOL/DME with 1% $LiNO_3$	0.5	1	150	150	97%
Powder-sintering derived 3D porous current collector for stable lithium metal anode	3D current collector	1 m LiTFSI in DOL/DME with 1% $LiNO_3$	1	1	160	160	98.3%
Graphene nested porous carbon current collector for lithium metal anode with ultrahigh areal capacity	carbon fiber cloth + ZnO	1 m LiTFSI in DOL/DME	1	12	60	720	98.5%
			2	12	40	480	98%
Graphene anchored on Cu foam as a lithiophilic 3D current collector for a stable and dendrite-free lithium metal anode	Graphene anchored on Cu foam	1 m LiTFSI in DOL/DME with 2% $LiNO_3$	0.5	1	150	150	98.60%
			2	1	250	250	97.40%
Uniform Li deposition regulated via three-dimensional polyvinyl alcohol nanofiber networks for effective Li metal anodes	three-dimensional nanofiber network structure	1 m LiTFSI in DOL/DME with 3% $LiNO_3$	1	1	200	200	98.60%
			3	1	200	200	97.40%
			5	1	200	200	87.70%
Hierarchically Bicontinuous Porous Copper as Advanced 3D Skeleton for Stable Lithium Storage	highly porous copper	1 m LiTFSI in DOL/DME with 1% $LiNO_3$	1	1	270	270	98%
			1.5	1	200	200	96%
			2	1	150	150	95%
			3	1	100	100	94%
Suppressing Li Metal Dendrites Through a Solid Li‐Ion Backup Layer	lithiated multiwall carbon nanotubes	1 m LiTFSI in DOL/DME	1	0.5	50	25	99.8%
Lithiophilic-lithiophobic gradient interfacial layer for a highly stable lithium metal anode	zinc oxide/carbon nanotube sublayer	0.6 M LiTFSI DOL/DME + 0.4 M $LiNO_3$	2	3	100	300	99.5%
Stretchable Lithium Metal Anode with Improved Mechanical and Electrochemical Cycling Stability	Stretchable Lithium Metal Anode	1 M LiTFSI in DOL/DME + 1wt% $LiNO_3$	1	1	176	176	97.50%
			2	1	48	48	96%
Pseudocapacitance Induced Uniform Plating/Stripping of	3D vertical graphene nanowalls	1 M $LiPF_6$ in EC:DEC 1:1 with 2 vol% FEC	0.5	1	250	250	97%

Li Metal Anode in Vertical Graphene Nanowalls	on nickel (Ni) foam (VGN/Ni)	1 M LiTFSI in DOL/DME with 0.2M $LiNO_3$	0.5	1	150	150	99%
In Situ Synthesis of a Lithiophilic Ag-Nanoparticles-Decorated 3D Porous Carbon Framework toward Dendrite-Free Lithium Metal Anodes	Lithiophilic Ag-Nanoparticles-Decorated 3D Porous Carbon Framework	1 M LiTFSI in DOL/DME + 2wt% $LiNO_3$	0.5	1	200	200	98%
			1	1	150	150	96%
Engineering stable interfaces for three-dimensional lithium metal anodes	3D electrode using ALD-coated hollow carbon spheres	1 M $LiPF_6$ in EC/DEC w/ VC and 10% FEC	2	1	100	100	96%
		1 M LiTFSi in DOL/DME with 5% $LiNO_3$	0.5	1	500	500	99%
Crumpled Graphene Balls Stabilized Dendrite-free Lithium Metal Anodes	Crumpled Graphene Balls	1 M LiTFSI in DOL/DME with 1 wt% $LiNO_3$	0.5	0.5	700	350	97.5%
Three-dimensional pie-like current collectors for dendrite-free lithium metal anodes	3D host	1 M LiTFSi in DOL/DME with 1 wt% $LiNO_3$	1	2	200	400	97%
Spatially uniform deposition of lithium metal in 3D Janus hosts	Janus 3D current collector	1 m LiTFSI in DOL/DME with 1% $LiNO_3$	0.2	1	100	100	99.5%
			1	1	100	100	99.1%
			2	1	100	100	97.6%

Li metal protection

Tile of literature	Strategy	Electrolyte	Current (mA cm^{-2})	Capacity (mAh cm^{-2})	Cycle #	Cumulative Capacity (mAh)	CE
An Artificial Solid Electrolyte Interphase with High Li-Ion Conductivity, Mechanical Strength, and Flexibility for Stable Lithium Metal Anodes	Cu_3N+SBR artificial SEI	1 M $LiPF_6$-EC/DEC (1:1 vol.) + 10 wt% FEC	1	1	100	100	97.40%
			0.25	0.5	150	75	98%
The Long Life-span of a Li-metal Anode Enabled by a Protective Layer Based on the Pyrolyzed N-doped Binder Network	Polyacrylonitrile protection	1 M $LiPF_6$-EC/DEC (1:1 vol.) + 5 vol% FEC	0.5	1	350	350	98%
Poly(dimethylsiloxane) Thin Film as a Stable Interfacial Layer for High-Performance Lithium-Metal Battery Anodes	Poly(dimethylsiloxane) artificial SEI	1 M $LiPF_6$-EC/DEC (1:1 vol.) + 2 wt% VC	0.25	1	200	200	93%
			0.5	1	100	100	90%
			1	1	100	100	89%
Volumetric variation confinement: surface protective structure for high cyclic stability of lithium metal electrodes	Al_2O_3 nano-powder	1 M $LiPF_6$-EC/DMC + FEC	0.5	1	50	50	97.60%
Interfacial Chemistry Regulation via a Skin-Grafting Strategy Enables High-Performance Lithium-Metal Batteries	Surface protection	1 M $LiPF_6$-EC/EMC/FEC (3:7:1 vol.)	0.5	1	200	200	98%
Electrochemical behaviors of a Li_3N modified Li metal electrode in secondary lithium batteries	Li_3N film on Li metal	1 M LiPF6-EC/DMC (1:1 wt.)	0.5	0.25	80	20	85%
Stabilizing Li/Electrolyte Interface with a Transplantable Protective Layer Based on Nanoscale LiF Domains	Nanoscale LiF Lithium protection	1 M $LiPF_6$-EC/EMC/DEC + 3% FEC	0.5	1	300	300	98%
Ultrathin Two-Dimensional Atomic Crystals as Stable Interfacial Layer for Improvement of Lithium Metal Anode	Hexagonal boron nitride and graphene on Cu metal	1 M $LiPF_6$-EC/DEC (1:1 vol.)	1	1	50	50	93%
			1	3	50	150	95%
			1	5	50	250	95%
Stabilizing Lithium Metal Anodes by Uniform Li-Ion Flux Distribution in Nanochannel Confinement	Polymide coating layer with nanochannels	1 M $LiPF_6$-EC/DEC (1:1 vol.)	1	1	40	40	89%
An Artificial Solid Electrolyte Interphase Layer for Stable Lithium Metal Anodes	Li_3PO_4 layer	1 M $LiPF_6$-EC/DMC/DEC (1:1:1 vol.)		1	10	10	95%
Regulating Li deposition at artificial solid electrolyte interphases	LiF coating	DOL/DME	0.5	1	90	90	99%
Coated Lithium Powder (CLiP) Electrodes for Lithium-Metal Batteries	Coated lithium powder electrodes	1 M $LiPF_6$-EC/DMC (1:1 vol.)	0.885	0.885	100	88.5	94.90%
High-Performance Lithium Metal Negative Electrode with a Soft and Flowable Polymer Coating	Adaptive Polymer Coating	1.0 m LiTFSI in DOL/DME with 1% $LiNO_3$	1	1	180	180	97%
Lithium Metal Anodes with an Adaptive "Solid-Liquid" Interfacial Protective Layer	Coating	1 m LiTFSI in DOL/DME with 1% $LiNO_3$	0.5	1	120	120	97.60%
Polymer Nanofiber-Guided Uniform Lithium Deposition	PAN coating	1 m LiTFSI in DOL/DME with 2% $LiNO_3$	1	1	120	120	97.9%

for Battery Electrodes							
Effects of Polymer Coatings on Electrodeposited Lithium Metal	Polymer Coatings	1 m LiTFSI in DOL/DME with 1% $LiNO_3$	0.5	1	10	10	99.13%
Regulating Li deposition at artificial solid electrolyte interphases	Nanoporous $\gamma-Al_2O_3$ membranes	1 m LiTFSI in DOL/DME with 1% $LiNO_3$	0.5	0.25	300	75	95%
An Armored Mixed Conductor Interphase on a Dendrite-Free Lithium-Metal Anode	mixed ionic/electronic conductor interphase	1.0 M $LiPF_6$ in EC-DEC (v/v=1:1)	0.5	1	50	50	96.30%
Combinatorial Methods for Improving Lithium Metal Cycling Efficiency	Zn Coating	1M $LiPF_6$ FEC:TFEC	1	1	100	100	99.1%
			1	3	100	300	99%
An ultrafast rechargeable lithium metal battery	organic/inorganic composite protective layer	1 M $LiPF_6$-EC/DEC (1:1 vol.) + 0.1 M $Mn(NO_3)_2$	3	6	150	900	94%
Novel ALD Chemistry Enabled Low-Temperature Synthesis of Lithium Fluoride Coatings for Durable Lithium Anodes	ALD LiF coating	1 m LiTFSI in DOL/DME with 2% $LiNO_3$	0.4	0.4	150	60	99.5%
			1	1	150	150	98.5%
A tin-plated copper substrate for efficient cycling of lithium metal in an anode-free rechargeable lithium battery	A tin-plated copper substrate	1 M $LiPF_6$ in FEC/EMC 1:4	0.5	0.5	40	20	92%
Chemically polished lithium metal anode for high energy lithium metal batteries	Chemically polished lithium metal anode	1 M $LiPF_6$ in EC/DEC	1	1	300	300	94.2%
Polymer–inorganic solid–electrolyte interphase for stable lithium metal batteries under lean electrolyte conditions	Reactive polymer composite derived SEI + 3D graphene oxide sheets	1 M $LiPF_6$ in EC/EMC (3:7 vol.) with 2% LiBOB	2	4	300	1200	99.1%
			2	2	750	1500	99.2%
			2	8	160	1280	98.6%
			1	1	200	200	99.3%
Core–Shell Nanoparticle Coating as an Interfacial Layer for Dendrite-Free Lithium Metal Anodes	SiO_2 PMMA core shell nanospheres	1 M $LiPF_6$-EC/DEC (1:1 vol.) SiO_2 core diameter 450 nm PMMA thickness 20 nm	0.5	2	50	100	87%
		1 M $LiPF_6$-EC/DEC (1:1 vol.) SiO_2 core diameter 550 nm PMMA thickness 10 nm	0.5	2	50	100	83%
		1 M $LiPF_6$-EC/DEC (1:1 vol.) SiO_2 core diameter 550 nm PMMA thickness 20 nm	0.5	2	50	100	81%
		1 M $LiPF_6$-EC/DEC (1:1 vol.) SiO_2 core diameter 550 nm PMMA thickness 10 nm	1	2	50	100	90%
			1	1	50	50	81%
			1	4	50	200	85%

Separator modification

Tile of literature	Strategy	Electrolyte	Current (mA cm^{-2})	Capacity (mAh cm^{-2})	Cycle #	Cumulative Capacity (mAh)	CE
High-capacity Rechargeable Batteries Based on Deeply Cyclable Lithium Metal Anodes	Slow release of $LiNO_3$	1 M $LiPF_6$-EC/DEC (1:1 vol.)	1	1	242	242	92.20%
			2	1	240	240	93.70%
			4	1	120	120	92.70%
			1	2	217	434	95.10%
			1	5	160	800	98.30%
			1	10	60	600	98.40%
			2	5	100	500	96.80%
			5	5	59	295	98.00%
			2	10	57	570	98.50%
			5	10	53	530	98.10%
Suppressing Lithium Dendrite Growth by Metallic Coating	Ultrathin Cu coated separator	1 M $LiPF_6$-EC/DEC (1:1 vol.) + 10wt% FEC +	0.4	0.5	300	150	95.60%

on a Separator		1 wt% VC	1	1	100	100	92.10%
A Thermally Conductive Separator for Stable Li Metal Anodes	Separator coated with Boron Nitride	1 M $LiPF_6$-EC/DEC (1:1 vol.)	0.25	1	100	100	94%
			0.5	1	100	100	92%
			1	1	100	100	88%
A novel ZnO-based inorganic/organic bilayer with low resistance for Li metal protection	PVDF-HFP/ZnO composite membrane	1 M $LiPF_6$ in 1:1 EC:DMC with 3 wt% FEC)	0.5	1	100	100	95.7%

Electrolyte and additives

Tile of literature	Strategy	Electrolyte	Current (mA cm^{-2})	Capacity (mAh cm^{-2})	Cycle #	Cumulative Capacity (mAh)	CE
Fluoroethylene Carbonate Additives to Render Uniform Li Deposits in Lithium Metal Batteries	FEC additives	1 M $LiPF_6$-EC/DEC (1:1 vol.) + 5 vol% FEC	0.1	0.5	100	50	98%
			0.5	0.5	100	50	90%
Synergism of Al-containing Solid Electrolyte Interphase Layer and Al-based Colloidal Particles for Stable Lithium Anode	$AlCl_3$ additive	1 M $LiPF_6$-EC/DMC/DEC (1:1:1 vol.) with $AlCl_3$ additive	0.5	2	150	300	98%
In Situ Plating of Porous Mg Network Layer to Reinforce Anode Dendrite Suppression in Li-Metal Batteries	$Mg(TFSI)_2$ additive	1 M $LiPF_6$-EC/DMC (1:1 vol.) + $Mg(TFSI)_2$	0.5	1	240	240	88%
			1	2	130	260	91%
			2	4	50	200	88%
A promising bulky anion based lithium borate salt for lithium metal batteries	LiTFPFB salt	1 M LiTFPHB-PC	0.5	0.5	50	25	80.60%
In-Situ Formation of Stable Interfacial Coating for High Performance Lithium Metal Anodes	Methyl viologen hexafluorophosphate	1 M $LiPF_6$-EC/DEC (1:1 vol.) + 1 vol% VC + 10 vol% FEC + 0.5 wt% MV	2	2	92	184	94.60%
Nanodiamonds suppress the growth of lithium dendrites	Nanodiamonds	1 M $LiPF_6$-EC/DEC (1:1 vol.) + ODA-functionalizd nanodiamond (0.41mg/mL)	0.5	0.5	12	6	96%
		1 M LiPF6-EC/DEC (1:1 vol.) + ODA-functionalizd nanodiamond (0.82mg/mL)	0.5	0.5	100	100	96%
A highly reversible room-temperature lithium metal battery based on crosslinked hairy nanoparticles	Crosslinked-Nanoparticle-Polymer-Composites electrolyte	CNPC in 1 M LiTFSI-PC + 1wt% $LiNO_3$ + 2 vol% VC	0.25	0.5	100	50	97.5%
Lithium Fluoride Additives for Stable Cycling of Lithium Batteries at High Current Densities	Addition of LiF salt	1 M $LiPF_6$-EC/DMC + 0.5 wt% LiF	0.25	1	120	120	90%
			0.5	1	120	120	86%
Guided Lithium Metal Deposition and Improved Lithium Coulombic Efficiency through Synergistic Effects of $LiAsF_6$ and Cyclic Carbonate Additives	$LiAsF_6$ + cyclic carbonate additives	1 M $LiPF_6$-PC + 2wt% VC + 2wt% $LiAsF_6$	0.2	0.347222223	10	3.47	96.7%
Dendrite - Free and Performance - Enhanced Lithium Metal Batteries through Optimizing Solvent Compositions and Adding Combinational Additives	LiTFSI - LiBOB/ carbonate dual - salt electrolyte	0.6 M LiTFSI + 0.4 M LiBOB + 0.6 wt% $LiPF_6$ + 2.0 wt% VC + 2.0 wt% FEC in EC/EMC (7:3 by wt.)	0.5	1	10	10	98.1%
In Situ Scanning Vibrating Electrode Technique for the Characterization of Interface Between Lithium Electrode and Electrolytes Containing Additives	AlI_3 additive	1 M $LiClO_4$-PC + 100 ppm AlI_3 + 0.5vol% 2-methylfuran	2	0.055555556	20	1.11111112	94%
Lithium metal protection through in-situ formed solid electrolyte interphase in lithium-sulfur batteries: The role of polysulfides on lithium anode	Polysulfides	0.1 M Li_2S_5 + 5% $LiNO_3$ in 1 M LiTFSI in DOL/DME	1	1	200	200	97%
Lithium metal stripping/plating mechanisms studies: A metallurgical approach	Pressure	1 M $LiPF_6$-EC/DMC (1:1 vol.)		2.7	10	27	90%
Effects of Some Organic Additives on Lithium Deposition in Propylene Carbonate	FEC Additive	1 M $LiClO_4$-PC + 5% FEC	0.5	0.083333333	30	2.5	80%
A bifunctional electrolyte additive for separator wetting and dendrite suppression in lithium metal batteries	Triblock polyether additive	1 M $LiPF_6$-PC + 0.2% P123		1	50	50	40%
Surface Condition Changes in Lithium Metal Deposited in Nonaqueous Electrolyte Containing HF by Dissolution-Deposition Cycles	HF additive	1 M $LiCF_3SO_3$-PC + 20 mM HF + 27 mM H_2O		1	100	100	60%
In situ scanning vibrating electrode technique for lithium	SnI_2 additive	1 M $LiClO_4$-PC/2Me-THF + 200 ppm SnI_2	2	0.2	20	4	80

metal anodes							
Electrochemical deposition of lithium metal in nonaqueous electrolyte containing $(C_2H_5)_4NF(HF)_4$ additive	$(C_2H_5)_4NF(HF)_4$ additive	1 M $LiCF_3SO_3$-PC	1	1	35	35	80%
The correlation between the cycling efficiency, surface chemistry and morphology of Li electrodes in electrolyte solutions based on methyl formate	Methyl formate solution and CO_2	1 M $LiAsF_6$ in DEC + methyl formate (0.5 vol.) under 6 atm CO_2	1	1.25	20	25	97.5%
Enhanced cyclability and surface characteristics of lithium batteries by Li–Mg co-deposition and addition of HF acid in electrolyte	Mg co-deposition and addition of HF acid	1 M $LiPF_6$-EC/DEC/DME + 0.05 M $Mg(ClO_4)_2$ + 0.3 ppm HF	1	0.4	100	40	50%
AC imepedance behaviour of lithium electrode in organic electrolyte solutions containing additives	Benzene additive	PC + 5 vol% benzene	1	0.1	20	2	78%
Concentrated dual-salt electrolytes for improving the cycling stability of lithium metal anodes	Concentrated dual-salt electrolytes	1M LiFSI +2M LiTFSI in DOL/DME	0.5	1	200	200	97.7%
Novel Concentrated Li[$(FSO_2)(n\text{-}C_4F_9SO_2)$N]-Based Ether Electrolyte for Superior Stability of Metallic Lithium Anode	Concentrated ether electrolyte	3 M LiFNSI in DOL/DME	0.5	1	180	180	97%
Novel dual-salts electrolyte solution for dendrite-free lithium-metal based rechargeable batteries with high cycle reversibility	Dual-salts electrolyte	0.5 M LiTFSI + 0.5 M LiFSI in DOL/DME	0.25	0.625	120	75	99%
Li_2S_5-based ternary-salt electrolyte for robust lithium metal anode	Ternary-salt electrolyte	Li_2S_5 ([S]=0.10 M)–$LiNO_3$ (1.0 wt%, ~0.15 M)-LiTFSI (1.0 M)	0.5	0.5	100	50	95%
The synergetic effect of lithium polysulfide and lithium nitrate to prevent lithium dendrite growth	Lithium polysulfide and lithium nitrate	0.18 M Li_2S_8 + 5 wt% $LiNO_3$ in DOL/DME	2	1	400	400	99.1%
High rate and stable cycling of lithium metal anode	High concentration electrolyte	4 M LiFSI-DME	0.2	0.5	500	250	99.1%
			1	0.5	500	250	98.5%
			4	0.5	1000	500	98.4%
			10	0.5	500	250	97%
Solubility-mediated sustained release enabling nitrate additive in carbonate electrolytes for stable lithium metal anode	nitrate nanoparticles encapsulated in porous polymer gel	0.5 M $LiPF_6$ in EC/DEC	1	1	200	200	98.1%
Passivation of Lithium Metal Anode via Hybrid Ionic Liquid Electrolyte toward Stable Li Plating/Stripping	Hybrid Ionic Liquid Electrolyte	2 M LiTFSI/Py13TFSI + DOL/DME	0.5	1	360	360	99.10%
Dual‐Layered Film Protected Lithium Metal Anode to Enable Dendrite‐Free Lithium Deposition	FEC	1 M $LiPF_6$-FEC	1	1	10	10	98.3%
Electrode Edge Effects and Failure Mechanism of Lithium Metal Batteries	High concentration electrolyte + no edge effect	LiFSI/DMC/BTFE=0.51:1.1:2.2 by mol.	0.5	1	10	10	99.4%
The behaviour of lithium electrodes in propylene and ethylene carbonate: The major factors that influence Li cycling efficiency	Electrolyte Additives	1.5 M $LiAsF_6$-PC	1.5	0.173611111	10	1.73611111	85%
		1.5 M $LiAsF_6$-PC + CO_2 saturation	1.5	0.173611111	10	1.73611111	93%
		1.5 M $LiAsF_6$-PC + storage over Al_2O_3	1.5	0.173611111	10	1.73611111	96%
Engineering Solid Electrolyte Interphase in Lithium Metal Batteries by Employing an Ionic Liquid Ether Double-Solvent Electrolyte with Li[$(CF_3SO_2)(n\text{-}C_4F_9SO_2)$N] as the Salt	Electrolyte Additives	1 M TNFSI in DOL/PI13FSI	0.5	1	300	300	98.70%
Tuning the electrolyte network structure to invoke quasi-solid state sulfur conversion and suppress lithium dendrite formation in Li–S batteries	Decreasing the solvent/salt molar ratio	G2:LiTFSI (0.8:1)	1	1	200	200	96.20%
A $LiPO_2F_2$/LiFSI dual-salt electrolyte enabled stable cycling of lithium metal batteries	Dual salt	0.5 M LiFSI+0.5 M $LiPO_2F_2$/DME	0.5	1	150	150	96.40%
$(CH_3)_3$Si-N[$(FSO_2)(n\text{-}C_4F_9SO_2)$]: An additive for dendrite-free lithium metal anode	$(CH_3)_3$Si-N[$(FSO_2)(n\text{-}C_4F_9SO_2)$]	1 M LiTFSI in DOL/DME with 5wt% TMS-FNFSI	0.25	0.5	200	100	98.60%
			0.5	1	100	100	97.30%
			1	2	100	200	96.50%
		2.5 M LiTFSI in DMC-BTFE	0.5	1	10	10	99.5%

High Voltage Lithium Metal Batteries Enabled by Localized High Concentration Electrolytes	Localized high concentration electrolytes	1.2 M LiTFSI in DMC-BTFE	0.5	1	10	10	99.3%
			1	1	10	10	99.4%
			3	1	10	10	98.9%
			5	1	10	10	92.6%
			0.5	1	200	200	99%
A Localized High-Concentration Electrolyte with Optimized Solvents and Lithium Difluoro(oxalate)borate Additive for Stable Lithium Metal Batteries	Localized high concentration electrolytes	1.2 M LiFSI in EC/EMC with BTFE + 0.15M LiDFOB	0.5	1	200	200	98.5%
Localized High-Concentration Sulfone Electrolytes for High-Efficiency Lithium-Metal Batteries	Localized High-Concentration Sulfone Electrolytes	LiFSI-3TMS-3TTE	0.5	1	150	150	98.80%
High-Efficiency Lithium Metal Batteries with Fire-Retardant Electrolytes	fire-retardant localized high-concentration electrolyte	1.2 M LiFSI/TEP-BTFE, 1:3 by mol	0.5	1	10	10	99.2%
			1	1	10	10	99.2%
			2	1	10	10	98.9%
			3	1	10	10	98.5%
Monolithic solid–electrolyte interphases formed in fluorinated orthoformate-based electrolytes minimize Li depletion and pulverization	Localized high concentration electrolytes	1 M LiFSI/DME-TFEO	0.5	1	10	10	99.5%
Enabling High-Voltage Lithium-Metal Batteries under Practical Conditions	Localized high concentration electrolytes	LiFSI-1.2DME-3TTE	0.5	1	300	300	99.3%
Lithium Difluorophosphate as a Dendrite-Suppressing Additive for Lithium Metal Batteries	Lithium Difluorophosphate	1 M $LiPF_6$ in EC/DEC + 0.15M LiDFP	1	1	40	40	98.3%
Combinatorial Methods for Improving Lithium Metal Cycling Efficiency	Electrolyte	1M $LiPF_6$ FEC:TFEC	0.6	0.444444445	50	22.22	75%
Fluorine-donating electrolytes enable highly reversible 5-V-class Li metal batteries	Fluorine-donating electrolytes	7 m LiFSI in FEC	0.25	0.5	400	200	99.6% max
			0.5	0.5	350	175	98.37% max
			1	0.5	300	150	98.02% max
Non-flammable electrolyte enables Li-metal batteries with aggressive cathode chemistries	non-flammable fluorinated electrolyte	1 M $LiPF_6$ in FEC/FEMC/HFE	0.2	1	500	500	99.2%
			0.5	2	400	800	99%
Effect of vinylene carbonate as additive to electrolyte for lithium metal anode	VC additive	1M $LiPF_6$-EC/DMC/DEC (1:1:1 vol.) + 2 wt% VC	0.6	0.444444445	50	22.22	75%
		1M LiBETI-EC/DMC/DEC (1:1:1 vol.) + 2 wt% VC	0.6	0.444444445	50	22.22	86%
		1 M LiTFSI-EC/DMC (1:1 vol.) +2 wt% VC	0.6	0.444444445	50	22.22	82%
		1 M $LiBF_4$-EC/DMC (1:1 vol.) +2 wt% VC	0.6	0.444444445	50	22.22	80%

Table S3. Cell Parameters of a 300 Wh kg^{-1} Li||SPAN Pouch Cell (Cell Dimensions: 70 × 41.5 mm).

Cell component	Cell parameters	
Cathode	discharge capacity (mAh g^{-1})	694
	active material Loading	90%
	total coating weight (mg cm^{-2} each side)	8.0
	area Capacity (mAh cm^{-2} each side)	5
	Al foil thickness (um)	15
	number of double coated layers	16
Li Anode	cell balance (N/P ratio)	1
	electrode thickness (single side) (um)	50
	Cu foil thickness (um)	8
Electrolyte	electrolyte/capacity (g Ah^{-1})	2
	weight (g)	6.192
Separator	Thickness (um)	20
Cell	voltage (V)	1.8
	capacity (mAh)	3096
	energy density (Wh kg^{-1})	307